Diversity of soluble salt concentrations on volcanic ash aggregates from a variety of eruption types and deposits

Mathieu Colombier[1]; Sebastian B. Mueller[2], Ulrich Kueppers[1], Bettina Scheu[1], Pierre Delmelle[3], Corrado Cimarelli[1], Shane J. Cronin[4], Richard J. Brown[5], Manuela Tost[4], and Donald B. Dingwell[1]

[1]Department of Earth and Environmental Sciences, Ludwig-Maximilians-Universität München, Germany; [2]Department of Geology and Geophysics, University of Hawaii at Mānoa, Honolulu, Hawaii, USA; [3]Université catholique de Louvain, Earth & Life Institute, Environmental Sciences, Belgium; [4]School of Environment, University of Auckland, New Zealand; [5]Department of Earth Sciences, Durham University, UK

Keywords

Ash aggregates, leaching, salt precipitation, particle binding, plume dispersal

Abstract

Ash aggregation is a common phenomenon in particle-laden environments of volcanic eruption plumes and pyroclastic density currents. Many of these initially fragile aggregates gain sufficient mechanical strength to remain intact after atmospheric transport and deposition. Several processes contribute to ash aggregate stability, including: electrostatic and hydrostatic bonding, ice formation and cementation by salt precipitates. Here, we compare leachate chemistry from aggregates from a variety of eruption and sedimentation conditions, ranging from dry magmatic eruptions with immediate deposition, to eruptions through seawater. The leachate data shows that the broad window of opportunity for aggregation and aggregate breakup may be used to qualitatively constrain suspended ash concentration and its temporal evolution. We show that aggregation rate and aggregate stability largely depend on the availability of external water and salt source. In particular, high humidity and extensive salt precipitation in seawater environments, such as during Surtseyan eruptions, promote high aggregation rates and aggregate stability, with accordingly accentuated proximal deposition and aggregate concentration in the deposits. On the other hand, low humidity and salt concentrations during dry magmatic eruptions promote less aggregation and more efficient aggregate break-up, explaining the rarity of aggregates in the deposits. These results have strong implications

for the ash budget in volcanic plumes and associated models of plume dispersal and related hazards.

Introduction

Ash aggregation is a common phenomenon associated with explosive volcanism. Volcanic ash particles in both eruptive plumes and pyroclastic density currents (PDCs) are believed to experience repeated contact with other particles (Saxby et al. 2018; Costa et al. 2006; Draxler and Hess 1997). Upon approach and contact, the physical forces of electrostatic or hydrostatic bonding (Alois et al. 2017; Mueller et al. 2016; Del Bello et al. 2015; Van Eaton et al. 2012; Costa et al. 2010; James et al. 2002; Gilbert and Lane 1994) may help to overcome rebounding forces and thereby enhance aggregate growth (Ennis et al. 1991). Only aggregates strong enough to survive atmospheric transport and deposition are preserved in the geological record. These can be used as conservative input parameter for residence time of suspended ash influencing ash dispersal (Folch et al. 2010). The adhesion forces of hydrostatic bonding (that is related to hydrogen bonding due to polarity of H_2O molecules) and electrostatic bonding are too weak for long-term aggregation ($<10^4$ nN, Salman et al. 2006), so that other mechanisms must stabilize new aggregates during transport and deposition. One key stabilization process is the precipitation of soluble salts in inter-particle voids (Mueller et al. 2016).

Several studies (e.g., Gilbert and Lane 1994; Kueppers et al. 2016) demonstrated the presence of salts in aggregates, and their importance in stabilizing aggregates has been demonstrated both experimentally and numerically (Mueller et al. 2017a, b). Both volcanic and environmental gases and fluids can drive salt precipitation on volcanic ash surfaces. Ayris et al. (2013, 2014) showed how the direct adsorption of volcanic gases such as SO_2, HCl or HF drive diffusion-driven salt precipitation. Also, salts form by condensation of acidic liquid droplets (or aerosols) on ash surfaces (Rose 1977; Hoshyaripour et al. 2014). During transport in volcanic plumes, ash particles may become partially- or fully-coated with aerosol droplets (Delmelle et al. 2005; Lathem et al. 2011) that are formed through the condensation of volcanogenic acid solutions of H_2SO_4, HCl and/or HF (Oskarsson 1980; Rose 1977). Such acidic liquid droplets condense on ash surfaces and may rapidly dissolve both glass and mineral constituents (Delmelle et al., 2007; Hoshyaripur et al. 2014). Capillary forces focus thin films of acidic liquids to particle-particle connection points within aggregates causing point-source dissolution (Mueller et al. 2017a, b). Subsequent evaporation of the liquid phase means that these contact points may be bridged between particles by nm- to µm-sized crystals of sulfate and halide salts

as the condensed liquid saturates. This type of salt cementation in volcanic ash aggregates occurs within a few seconds during experimental observations (Mueller et al. 2016). We note that low Reynolds numbers were used in these experiments (8-28, see Mueller et al. 2016). These are more applicable to dilute parts of PDCs, such as co-PDC plumes, rather than energetic basal parts (cf. Mueller et al. 2016). On the other hand, these experiments also computed a range of viscous Stokes numbers (St, Ennis et al. 1991) with values ranging between 10^0 and 10^2.

Laboratory experiments suggest a minimum salt concentration of 1800 ppm for efficient cementation of ash aggregates (Mueller et al. 2016). However, natural system salt concentrations involved in aggregate cementation are poorly constrained. This is partly because aggregates are sampled too long after primary deposition so that initial salts may be removed or re-crystallized and replaced during weathering, diagenesis or hydrothermal processes. Furthermore, several factors influence the efficiency of aggregation in nature, including (but not limited to): (1) ash granulometry (fraction of fine ash); (2) available humidity; (3) eruption "acidity" and (4) suspension conditions (e.g., Brown et al. 2012; Mueller et al. 2017a, b; Mueller et al. 2018).

In this study we quantify and compare the salt concentrations in natural ash aggregates across different eruptive settings. To explore conditions with a range of humidity and variable possible sources of salts we chose four case study volcanic ash/aggregate settings: (1) "low-salt" dry eruption and dry atmosphere; the 29 December 2013 eruption of Chaparrastique (San Miguel, El Salvador) volcano in a dry atmosphere; (2,3) "intermediate salt" in subaerial eruptions within a humid tropical atmosphere and with involvement of external water; the August 2006 Tungurahua eruption in Ecuador (Douillet et al. 2013; Kueppers et al. 2016) and a 2010 dome collapse event at Soufrière Hills, Montserrat (Stinton et al. 2014; Burns et al. 2017); and (4) "high salt" shallow submarine (Surtseyan) 2015 eruption of the Hunga Tonga-Hunga Ha'apai volcano (Colombier et al. 2019). We use the comparison of these settings to explore the variety of possible aggregation processes and relate this, in-turn, to the quantification of suspended ash concentrations during different types of eruption.

Case studies

Chaparrastique (San Miguel) volcano

Chaparrastique is a composite volcano in central-eastern El Salvador with its Summit at 2130 m above sea level (a.s.l). The 29 December, 2013 eruption produced a 9 km-high eruption column that dispersed ash to the west of the volcano (Scarlato et al. 2017). The eruption occurred during the dry season, on a nearly cloudless day, and video footage of the eruption, shot at distances of 8 km, indicates that the eruption commenced with a discrete explosion that rained tephra and ballistics over the summit. This was shortly followed by a larger explosion that produced a pyroclastic density current that travelled ~500 m down the flanks of the volcano before lofting (Scarlato et al. 2017). The eruption then transitioned to a phase characterized by a quasi-steady eruption column that dispersed scoria and ash to the west. Ash lofted from the pyroclastic density current drifted west across the flanks of the volcano and rained out ash aggregates over the western flank. The early explosions may have been driven by interaction between rising magma and groundwater/hydrothermal system in the subvolcanic structure (Scarlato et al. 2017). The aggregates form a framework-supported layer of less than 1-cm thick at the base of the tephra fall deposit. Aggregates represent only 5-10 wt% of the total ash deposit, and were sampled by us in late March/early April 2014.

Tungurahua volcano

Tungurahua volcano has its summit at 5017 m a.s.l. and is characterized by a humid tropical atmosphere. We sampled aggregates from the August 2006 eruption was a significant climatic point during an eruptive cycle that started in 1999 (Eychenne et al. 2012; Wright et al. 2012). This dry magmatic eruption occurred during poor weather/visibility between the 16 and 17 August and based on geophysical data lasted for ~8 hours (Kelfoun et al. 2009) with estimated plume heights of 6 to 13 km (Steffke et al. 2010). PDCs generated by column collapse (Steffke et al. 2010) occurred down the NW- and W-flank of the volcano (Douillet et al. 2013). At few locations, the PDCs interacted with the Chambo River at 2000 m a.s.l, locally damming the river for few hours (Kueppers et al. 2016). Aggregates were observed exclusively at the top (fines-poor, clast-supported lapilli tuff) of the 10 meter-thick and commonly massive ash lapilli tuffs, being limited to the top 50 cm of the stratigraphy where they represent less than 5 wt% of the deposit (Kueppers et al. 2016). These aggregates were sampled in August 2009.

Soufrière Hills volcano

Soufrière Hills volcano, 1050 m a.s.l., began a new cycle of activity characterized by dome extrusion punctuated by Vulcanian explosions triggered by dome collapse in 2010 (Stinton et al. 2014). On 11 February 2010 at 15:52 (UTC) a northward-directed partial dome collapse (50 × 10^6 m^3) occurred triggering PDCs that travelled about 1 km offshore and added about 1 km^2 of land to the island (Stinton et al. 2014). Through entering the ocean and triggering steam explosions, these PDCs produced co-PDC plume deposits containing abundant accretionary lapilli (Stinton et al. 2014), which were used for this study. Hence, these accretionary lapilli deposits are thought to be at the salt rich end of the spectrum, due to their interaction with ocean water. An extensive description of this event and its deposits was carried out by Stinton et al. (2014). The aggregates analyzed were sampled from Mueller et al. (2018) from the Unit III which was a 10 cm thick fall layer, underlain and overlain by massive PDC deposits. The abundance of aggregates decreases from 24 to 2 wt% with increasing distance from the sea (Burns et al. 2017).

Hunga Tonga- Hunga Ha'apai tuff cone

The Hunga Tonga- Hunga Ha'apai tuff cone was generated by a series of Surtseyan eruptions that started from a vent at a depth of ~150 m on the floor of the Pacific Ocean 1 km offshore of the islands of Hunga Tonga and Hunga Ha'apai during late 2014-early 2015 (Cronin et al. 2017). In a similar fashion to Surtsey (Kokelaar 1986; Cole et al. 2001), the Hunga eruptions progressively became emergent with the latest phases occurring within a water-filled subaerial crater (Cronin et al. 2017), with the deposit being divided into nine units (U1 through U9). Cronin et al (2017) reported a "drying" process during the emergent phase with a gradual decrease in the degree of water-magma interaction. The aggregates consist of scoriaceous lapilli clasts surrounded by ash rims (Colombier et al. 2019), which were sampled on the flanks of the tuff cone (Colombier et al. 2018). Six samples from six different stratigraphic units in the cone were collected during November 2015. Four samples, HH35, HH33, HH28 and HH23, were collected on the south-western flanks ~0.3 km from the center of the vent (in units U1, U3, U6 and U7). Instead, sample HH41 was collected on the south-west crater rim (<0.2 km from the vent) and corresponds to unit U9; and HH50 was sampled 1.4 km to the north of the vent center on the northern coastline and corresponds to the uppermost part of unit U6. Sample HH50 differs from the other samples as it is more distal and consists of an ash-rich layer with few

lapilli and might represent a more energetic eruptive pulse. The stratigraphic units studied here represent a portion of the emergent phase of the eruption leading to the building of the tuff cone. Although the water depth likely decreased during the eruptive sequence, the vent remained below sea level throughout the entire eruption, yet became isolated from the ocean at the end of the eruption (Cronin et al. 2018; Garvin et al. 2018). The water in the eruptive vent was mainly seawater, possibly chemically modified by interaction with the vent system, rain-fall runoff and leachates from the growing cone around it. In this regard, the tuff cone was subject to significant rain immediately after the cessation of eruptive activity in January 2015, leading to a well-developed erosional rill network (Cronin et al. 2017). Surface run-off may have reduced efficient percolation of rain water so that these samples appear only weakly leached. Aggregates are ubiquitous in the deposit, making up >90 wt% of the lapilli fraction (Colombier et al. 2019).

Methodology

Field work and sampling of the aggregates from Chaparrastique volcano were conducted in late March/early April 2014 before the deposit had been washed out by rain. Aggregates were sampled at a distance of ~1 km from the vent in the western flank. The internal structure and grain size of these aggregates were analyzed using back-scattered electron images (SU 5000 Schottky FE-SEM, HITACHI). Aggregates from other volcanoes were available from previous studies.

Aqueous leaching was used to determine surface salt concentration of ash aggregates from the different deposits. For each volcano, use of several aggregates was necessary in order to collect enough ash particles for the leaching analysis. We mechanically crushed aggregates and immersed fine to coarse grained ash particles in deionised water for one hour at solid:solution ratios of 1:100, 1:500 and 1:1000 (Table 1). For Soufrière Hills and Tungurahua volcanoes, we also analyzed non-aggregated material (loose matrix ash) in which the aggregates were embedded. Water extracts were filtered through a 0.2 µm cellulose-acetate membrane filter and analyzed for Cl^- and SO_4^{2-} in a Dionex 2000 ion chromatograph with an IonPac AS14 anion exchange column at the Université catholique de Louvain, Belgium. Concentrations of Al, Ca, Fe, K, Mg, Mn, and Si in leachate solutions were also determined by inductively coupled plasma atomic emission spectrometry (ICP-AES) at the Université catholique de Louvain. Short-term analytical precision (repeatability) is better than 5% for the ion chromatography and ICP-AES analyses.

In addition, we performed chemical mapping and morphological observations on the ash particles from various aggregates from sample HH33 of Hunga Tonga-Hunga Ha'apai using a Hitachi SU 5000 Scanning electron microscope (SEM) at Ludwig Maximilian University of Munich, Germany. We carefully removed the ash grains from these aggregates in order to avoid complete disaggregation and to preserve particle clusters with binding salts. Five of these particle agglomerates were chemically mapped.

A forward model was used to predict the sequence of salts precipitating during equilibrium evaporation of seawater with an average composition (Stumm and Morgan 1996). The calculations were performed with the open-source geochemical code PHREEQC 3.4 and using Pitzer's equations for solute activities at high ionic strength (Parkhurst and Appelo 1999) at a temperature of 70°C. The model allows precipitation (and possibly redissolution) of carbonate, sulfate and chloride salts, including anhydrite ($CaSO_4$), gypsum ($CaSO_4.2H_2O$), halite (NaCl), sylvite (KCl), bischofite ($MgCl_2.6H_2O$), glauberite ($Na_2Ca(SO_4)_2$), kieserite ($MgSO_4:H_2O$), polyhalite ($K_2MgCa_2(SO_4)_4:2H_2O$), hexahydrite ($MgSO_4:6H_2O$) and epsomite ($MgSO_4:7H_2O$).

Results

Aggregate types and characteristics

At Chaparrastique, the whitish aggregates are up to 10 mm in diameter and predominantly consist of poorly-structured ash pellets with few armored lapilli. The ash particles in these agglomerates range in size from ~ 1 to 400 µm in diameter. At Tungurahua volcano, the aggregates are up to 8 mm in diameter and consist of pellets pyroclasts made of grains ranging between <1-200 µm in diameter (Mueller et al. 2018). Aggregates at Soufrière Hills were described in detail by Burns et al. (2017) and further analyzed by Mueller et al. (2018) for particle size distribution. All are accretionary pellets with concentric structure and densities (ρ) and porosities (Φ) of 1300-1900 $kg.m^{-3}$ and 0.3-0.5, respectively (Burns et al. 2017). The aggregates range in diameter between 5 and 11 mm with ash grain sizes typically <200 µm (Mueller et al. 2018). Aggregates at the Hunga Tonga- Hunga Ha'apai tuff cone are essentially juvenile lapilli surrounded by an ash rim. Such particles would be termed "coated particles" using the nomenclature of Brown et al. (2012). However, we recently showed that a significant fraction of the ash grains from the rim were formed in situ by granulation of the core caused by thermal stress rather than by aggregation of external ash particles (Colombier et al. 2019). This

means that ash encasement is not always diagnostic of ash aggregation in the deposits from Surtseyan eruptions. Additional aggregation of external particles was however not ruled out. Hereafter, we will use the term aggregate for simplicity but it should be kept in mind that the formation mechanism of ash rims during Surtseyan eruptions may differ from other cases. The density and porosity of the aggregates are largely controlled by those of the central lapilli with values of ρ and Φ ranging between 300-1800 kg.m^{-3} and 0.35-0.89, respectively. The size of the aggregates at Hunga Tonga- Hunga Ha'apai varies between 2 and 5 mm with ash particles typically smaller than a few hundreds of µm (Colombier et al. 2019).

Leaching analysis

The raw data of concentrations for anions and cations in aggregated and non-aggregated material analyzed are given in Table 1 and are summarized for all aggregates in Figure 1. The concentrations of Cl^-, Na, $SO4^{2-}$, Ca, Mg and K evolve in a similar pattern between the aggregates from different settings and typically increase between our sites in the order: Chaparrastique < Tungurahua < Soufrière Hills < Hunga Tonga-Hunga Ha'apai (Fig. 1). In all cases, leachage concentrations are systematically higher in the aggregates than in non-aggregated ash (Table 1).

SEM observations and chemical mapping

Chemical mapping of aggregates from the HH33 sample of Hunga Tonga-Hunga Ha'apai, that had the highest leachate concentrations (Table 1), reveals the presence of several different salt phases at the ash surface and at the contact between ash particles (Fig. 2). Chemical mapping and crystal form were used for identification. The most abundant salts are NaCl and Ca_2SO_4, with KCl and $MgCl_2$ being much less abundant. NaCl and $CaSO_4$ crystals are the coarsest, ranging between 5-50 µm, while the less common salts are <5 µm in diameter. Relationships of 1:1 for the molar concentrations of NaCl and $CaSO_4$ confirms the SEM observations that these are the most abundant at Hunga Tonga-Hunga Ha'apai (Fig. 3). No similar stoichiometric trend is observed for the molar concentrations of other anion-cation pairs at Hunga Tonga-Hunga Ha'apai.

Model of salt precipitation

The evolution of the saturation state of seawater with respect to carbonate, sulfate and chloride salts during evaporation is shown in Figure 4. Calcite precipitates immediately upon evaporation. Anhydrite starts to precipitate at a concentration factor of around three (i.e. after ~24% of evaporation), followed by halite at a concentration factor of ~11 (i.e. after ~91% of evaporation) and then glauberite. Sylvite and kieserite precipitate when evaporation is almost complete (after >98% of evaporation).

Discussion

We first consider Surtseyan eruptions and how salt concentrations may evolve during progressive emergence and "drying" of eruptions. Secondly, we examine the process of salt precipitation on ash surfaces for a spectrum of "dry or low-salt" to "intermediate" and "wet or high-salt" eruption types. Finally, we generalize our findings to propose a conceptual model linking salt precipitation to eruptive scenario and the implications for ash dispersal and ash fall hazards.

Salt precipitation during Surtseyan eruptions

The concentrations of Na, Cl^-, Ca, $SO4^{2-}$, Mg and K are higher in aggregates from Hunga Tonga-Hunga Ha'apai than for Soufrière Hills, Tungurahua and Chaparrastique (in this order). To our knowledge, the maximum concentrations in Na, Cl^- and K found in these aggregates are, to date, the highest values found by leaching analysis of volcanic material (see Witham et al. 2005 and Ayris and Delmelle 2012 for compilations).

Diagrams comparing the concentrations of these anions and cations allow us to represent the traces of evaporation of seawater brines (Babel and Schreiber 2014). We observed a 1:1 relationship for the molar concentrations of Na-Cl and Ca-SO_4, consistent with NaCl and $CaSO_4$ seen in SEM (Fig. 3). Although K-Cl and Mg-Cl salts were observed during SEM analysis, their contribution to the total Cl^- content is negligible because of their low volumetric concentration (Fig. 2).

The Hunga Tonga-Hunga Ha'apai aggregates were sampled 10 months after deposition. There must have been some rainfall leaching so that the reported values are conservative estimates of primary salt precipitation in a volcanic plume, which will be favored by the temperature, salinity and humidity conditions during a Surtseyan eruption. A significant amount of seawater is contained in Surtseyan plumes and the high thermal budget likely drives it to rapidly boil, evaporate and concentrate into a pervasive brine causing salt precipitation. Hovland et al. (2006) showed that evaporation associated with boiling is rapid and highly productive. The extreme conditions of salinity, humidity, temperature, and high mobility of the seawater in Surtseyan settings probably contribute to the extensive salt precipitation observed here. Salts likely precipitate in the brine-soaked aggregates while they remain in the plume. Further, aggregates once formed could be re-coated by brine during transport in the plume, as well as after deposition. Once deposited, further burial by wet tephra accumulating above may cause brine to percolate downwards. In this way successive episodes of evaporation and precipitation could explain the concentrations in excess of those of seawater (Table 1). Additional primary salt precipitation by gas scavenging likely occurs but appears to be overwhelmed by seawater evaporation-induced precipitation.

The equilibrium evaporation calculations, leachate data and SEM analyses all point to the presence of $CaSO_4$ and NaCl salts in the ash aggregates. As illustrated in Figure 4, precipitation of sulfate and chloride salts on the ash surfaces required between 20 and 90 % of evaporation of seawater droplets. Although the model results predict that calcite is stable, carbonate salts were not observed in the ash aggregates. In contrast to sulfate and chloride salts, the low-pH conditions imparted by the volcanic gas condensates to the liquid phase within the eruption plume probably prevented precipitation/preservation of carbonates. Minor amounts of potassium chloride salts are shown in the SEM analysis, consistent with the modelled appearance of sylvite after almost complete brine evaporation (Fig. 4).

Variations in the anion and cation concentrations through the eruptive sequence also show the dominance of primary seawater evaporation during the Hunga Surtseyan eruption (Fig. 5). Secondary depletion of salts due to dissolution by rainwater alone cannot explain why some stratigraphic units are depleted and others not. Figure 5 shows an overall decrease of Na and Cl^- contents through the eruptive sequence (with the exception of sample HH50 from unit 6 which is enriched in these elements). The evolution of Ca and SO_4^{2-} is similar except for the last (highest) stratigraphic level sample, unit 8, which is enriched in $CaSO_4$.

This concentration pattern might reflect: (i) variable volumes of seawater involved during each eruptive phase sampled here; (ii) variable efficiency of seawater evaporation during the eruption sequence; or (iii) changes in the seawater composition. As the eruption progressed, it clearly became emergent (Cronin et al. 2017), thus less and less seawater was entrained in the plume. On the one hand, this "drying" process favors more efficient seawater evaporation because the particles stay hotter for longer due to the lower water:pyroclast ratios. However, the lower volumes of seawater entrained in the plume during emergence are likely responsible for the overall decrease in salt concentrations with height of the stratigraphy. These results hence suggest an overall decreasing degree of magma-water interaction during progressive emergence, in agreement with Cronin et al. (2017).

It was also observed from detailed studies of eruption footage of the Hunga Tonga-Hunga Ha'apai eruption (Taniela Kula; pers. comm.) that there were repeated partial collapses of the southern flank of the tuff cone and re-opening of the crater to the sea during the eruption. This likely caused sporadic renewed entry of seawater explaining why some intermediate units could be enriched in salts (e.g., sample HH50; Fig. 5). That the uppermost stratigraphic unit (sample HH41; Fig. 5) has a higher $CaSO_4$/NaCl than other units could also be due to rainfall leaching and the higher relative solubility of NaCl. Additional influences for these observed variations could be related to eruption of any hydrothermally-altered materials from the conduit as the eruption progressed. However, this does not appear to be the case at Hunga, because no evidences of hydrothermal clasts were found in any of the tephras.

Similar S- and Cl- bearing sea salts were reported within Soufrière Hills aggregates and likely further promoted aggregate cementation in the Co-PDC plumes (Burns et al. 2017). Morgavi et al. (2019) also recently proposed that high concentrations of seawater salts had a strong influence on aggregate cementation and resistance to breakage during the 7000 yrs. BP eruption of Secche di Lazzaro in Italy.

Salt precipitation and implications for aggregates in other settings

Our data show that precipitation occurs in a range of eruptive scenarios, from dry eruptions with only atmospheric humidity available for aggregation, to an oversupply of water during a Surtseyan eruption and resulting tephra-brine interaction (Fig. 6). Intermediate cases involve subaerial eruptions involving groundwater or PDCs entering the sea. Using our quantitative

dataset of salt concentrations in volcanic ash aggregates, we estimate here the minimum salt concentration needed for cementation.

Aggregates are preserved in the deposits from all eruptions examined, even with low total salt concentrations. With only <100 ppm for the "low-salt" Chaparrastique aggregates this is far lower than the threshold needed for aggregation suggested by laboratory-scale experiments (>1800 ppm; Mueller et al. 2016). For Chaparrastique volcano (salt-poor setting), the low salt concentrations are likely produced by the interaction of volcanic gas with atmospheric humidity or groundwater. We can also show that aggregate material has higher salt concentrations than non-aggregated free particles from the surrounding matrix in which the aggregates are embedded. This may reflect that the distribution of salts in the plume/PDC is not homogenous and permanent aggregation may only occur in particles in the salt-concentration zones. It may represent particular spatial mechanism for concentrating salts during an eruption (e.g., explosive interactions at the margins of a conduit or at the outer margins of a PDC entering water). Alternatively, it may represent short-lived conditions during an eruption as magma-water ratios vary or as vent conditions and atmospheric conditions change.

A minimum salt volume is therefore required to produce aggregates that survive transport and deposition. The ratio of aggregated to non-aggregated material might be related to the eruptive setting (amount of external water and salt source), the abundance and nature of the volcanic eruptive gas phase and secondary processes such as rain water influencing the salt content in the tephra after deposition. Additional factors such as the amount of degassing, the intensity of the eruption, the grain size distribution, the degree and duration of interaction of the tephra with volcanic gas, the occurrence of hydrothermal alteration prior to an eruption and the presence of a crater lake might also control the amount of salt precipitation and the aggregate stability (Armienta et al. 2002; Cronin et al. 2003).

Regarding the high salt concentrations found here for a seawater setting, we stress that high values of SO_4^{2-} and Cl^- have also been reported at other volcanoes (Figure 1). As an example, Cronin et al. (2003) found SO_4^{2-} contents of up to 31000 ppm in tephra layers from phreatomagmatic phases of the 1995-1996 Ruapehu eruption. Recently, Damby et al. (2018) reported the highest values for SO_4^{2-} ever found in volcanic leachates, with concentrations of up to 85000 ppm being recorded in ash deposits from the 2018 Kilauea eruption. The high concentrations in the cases of Ruapehu were attributed to the presence of an acidic crater lake and hydrothermal alteration prior to the eruption (Cronin et al. 2003). In the case of Kilauea, the very high values for SO_4^{2-} may partly be explained by the massive sulfur dioxide (SO_2)

emissions (of up to 50,000 tons per day; Neal et al. 2018) leading to chemical reactions between ash and the SO_2-rich plume causing the formation of calcium sulfates. The highest Cl^- values after those presented here for Hunga Tonga-Hunga Ha'apai were found in ash samples from Irazú volcano in Costa Rica (Taylor and Stoiber 1973). These high concentrations at Irazú might be explained by solfataric alteration (Taylor and Stoiber 1973) and/or enrichment by rain or the presence of a crater lake (Murata et al. 1966).

Implications for ash plume dispersal modelling and natural hazards

One of the key unknowns regarding aggregation in ash plume dispersal models involves aggregate break-up processes. Currently, models regard all aggregates as ash material which is quantitatively removed from the atmosphere (Folch et al. 2010). However, both experimental approaches (Mueller et al. 2017a, b) and *in-situ* field observations (Taddeucci et al. 2011; Bonadonna et al. 2011; Bagheri et al. 2016) clearly demonstrate the fragile nature of aggregates. Thus, we must infer that only a fraction of aggregates will be deposited as such. Whereas the process of aggregation can happen without any salt but with the mere presence of humidity (Mueller et al. 2016; Van Eaton et al. 2012; Schumacher and Schminke 1991; Gilbert and Lane 1994), the stability of aggregates, and therefore preservation chances increase with the amount of salts present as cementation agent. Experiments have shown that both the amount and presence of soluble salt compounds on ash surfaces can be derived from various eruption parameters, such as degassing rate or magma chemistry (Ayris et al. 2013, 2014; Delmelle et al. 2018).

Our study is the first to cover such a wide range of possible salt concentrations in volcanic ash aggregates, which represent a wide variety of eruptive settings as well as degrees of fresh and/or saltwater involvement. These data combined with recent experimental results (Mueller et al. 2017a, b), thus provide a resource for the consideration of aggregate stability and break-up in ash plume dispersal modelling. In experimental results, only about 50 wt.% of ash aggregates survived impact at terminal fall velocity at salt concentrations of 2000 ppm. Only at concentrations exceeding 50000 ppm, did 100 wt.% of ash aggregates survive impacts at terminal fall velocities. These experimental results are consistent with our observations on natural deposits. At Chaparrastique and Tungurahua, aggregates represent a low portion of the fall deposit (5-10 wt%), likely indicating both a lower aggregation rate related to low humidity, and a lower stability and higher break-up of the aggregates induced by the low salt

concentrations. On the other hand, all lapilli formed during the Surtseyan eruption at Hunga Tonga-Hunga Ha'apai preserved ash rims after deposition. Although some particles might have been lost from the ash rims, this suggests that stability of these aggregates comes close to 100 % due to the extremely high salt contents (tens of thousands of ppm), a conclusion which is also in agreement with the experiments of Mueller et al. (2017a, b). At Soufrière Hills, Burns et al. (2017) demonstrated that the abundance of aggregates decreases from 24 to 2 wt% as distance from the sea increases, further illustrating the role of sea salt concentration on the cementation and preservation of aggregates in the deposits. However, it is important to note that in all of these natural settings, additional parameters such as duration of transport, settling velocity, grain size and morphology of the aggregates, as well as the time of sampling after deposition, might influence the preservation of the aggregates during transport and deposition, and the salt concentrations. Additional data is therefore required to clearly quantify the link between salt concentration and aggregate abundance in natural deposits.

This study highlights the necessity for ash plume models to treat break-up processes of ash aggregates differently in distinct volcanic settings. Aggregates from eruptions that do not have any significant external salt source involved such as seawater, crater lake or hydrothermal systems (Cronin et al. 2003; Witham et al. 2005), exhibit salt concentrations well below 1000 ppm (Chaparrastique, Tungurahua, see Fig. 1). Paired with experimental results, this means that aggregates found in these deposits represent only a portion of the original number formed in the plume. Consequently, we infer that only a portion of aggregates incorporated in numerical ash plume models are actually removed from the atmosphere by aggregate deposition. The remaining portion is likely to stay airborne and become re-entrained into the dispersal process. Considering the volcanic setting, and in particular the humidity and abundance of external salt sources, will help to estimate the order of magnitude of aggregation rate, salt concentration and subsequent aggregate abundance and stability in volcanic plumes. Real time leaching analysis of ash and aggregates during eruptive crises might thus provide a valuable tool for plume forecast modelling, especially regarding the efficiency of atmospheric ash removal through aggregation. We anticipate that our new findings may thus represent a resource for the consideration of eruption source parameters (ESPs, Mastin et al. 2010) in ash dispersal modelling in which break-up processes in ash plume modelling, while being recognized, have not yet been quantified (Folch et al. 2010).

Finally, our results can also be useful to efforts to constrain the concentrations of soluble salts in a range of eruptive settings for the analysis of secondary remobilization of these salts which affects water resources, agriculture and human health (Damby et al. 2018). After

deposition, the ash deposits can interact with water leading to dissolution of the salts causing, for instance, contamination of drinking water (Damby et al. 2018). Here, the survival of ash aggregates is a constraint that contributes to the accurate forecasting of such secondary risks.

Conclusion

We here move towards a general, data-driven model for the process of particle binding by salt formation that covers a wide spectrum of eruptive scenarios ranging from dry, salt-poor magmatic eruptions to high humidity, salt-rich Surtseyan eruptions (and including intermediate cases). Key findings of our study include:

1. Variations in salt concentrations during volcanic eruptions can result from fresh and/or saltwater precipitation, gas scavenging, hydrothermal alteration and/or interaction with rain water.
2. An increase in the amount of salt sources in the vicinity of the vent or the transported tephra may lead to a dramatic increase in salt concentration promoting a greater stability of the aggregates.
3. The formation and survival of aggregates are ubiquitous during Surtseyan eruptions occurring in seawater due to both the high humidity and pervasive salt precipitation during such eruptions. This was confirmed by the very high salt concentrations found in the aggregates from the Hunga Tonga- Hunga Ha'apai 2014-2015 Surtseyan eruption.
4. The concentration of salts varies with stratigraphic height in tuff cones, with an overall reduction in salt content. This might reflect the progressive emergence during Surtseyan eruptions and decreasing volumes of seawater involved with time.
5. At a given volcano with specific aggregate characteristics and time of sampling after deposition, aggregates contain systematically more salts than non-aggregated particles. This implies that aggregates will only survive up to deposition when they contain a sufficient amount of salts.

Future studies focusing on a quantitative correlation between humidity, salt concentration and aggregate abundance in volcanic plumes and associated deposits will allow establishment of a link between volcanic eruption style (controlling grain size, abundance and nature of volcanic gas, suspension conditions), volcanic setting (controlling external salt sources and humidity), and aggregate abundance and preservation in volcanic plumes. This knowledge, coupled with systematic real time leaching analysis during volcanic eruptions may provide key

information on the concentration, stability and longevity of aggregates to be incorporated in ash plume dispersal models with far reaching implications for hazards related to populations and air traffic. Our results suggest that water and salt-rich volcanic settings, such as those during Surtseyan eruptions, will favor higher aggregate concentration and stability in volcanic plumes, likely enhancing proximal tephra deposition. Real time measurements of salt concentrations in shallow subaqueous environments could also shed light on the possible evolution toward dry magmatic phases during emergent phases.

Acknowledgements

MC and DBD acknowledge support from an ERC Advanced Grant (Explosive Volcanism in the Earth System: EVOKES - 247076). UK and SM acknowledge financial support by the European Commission (FP7-MC-ITN grant number 607905: VERTIGO). UK acknowledges financial support from grant KU2689/2-1 from the Deutsche Forschungsgemeinschaft. SJC and MT acknowledge funding support from the School of Environment and the Faculty Development Research Fund of the University of Auckland. MC and SBM are grateful to Koni for inspirational thoughts about this paper. We also thank the editor Andrew Harris, the associate editor Laura Pioli as well as Eduardo Rossi and an anonymous reviewer for discussions that contributed to substantial improvement of our initial manuscript.

References

Alois S, Merrison J, Iversen JJ, et al. (2017) Contact electrification in aerosolized monodispersed silica microspheres quantified using laser-based velocimetry. J Aerosol Sci 106:1–10. doi: 10.1016/j.jaerosci.2016.12.003

Armienta MA, La Cruz-Reyna SD, Morton O, et al. (2002) Chemical variations of tephra-fall deposit leachates for three eruptions from Popocatépetl volcano. J Volcanol Geotherm Res 113:61–80. doi: 10.1016/S0377-0273(01)00251-7

Ayris PM, Delmelle P (2012) The immediate environmental effects of tephra emission. Bull Volcanol 74:1905–1936. doi: 10.1007/s00445-012-0654-5

Ayris PM, Lee A, Wilson K, et al. (2013) SO_2 sequestration in large volcanic eruptions: high-temperature scavenging by tephra. Geochim Cosmochim Acta 110:58–69. doi: 10.1016/j.gca.2013.02.018

519 Ayris PM, Delmelle P, Maters EC, et al. (2014) HCl uptake by volcanic ash in the high
520 temperature eruption plume: mechanistic insights. Geochim Cosmochim Acta 144:188–
521 201. doi: 10.1016/j.gca.2014.08.028

522 Babel M, Schreiber BC (2014) Geochemistry of evaporites and evolution of seawater:
523 Treatise on Geochemistry. Second Edition, Elsevier Ld. 488–544. doi:10.1016/b978-0-
524 08-095975-7.00718-x

525 Bagheri G, Rossi E, Biass S, et al. (2016) Timing and nature of volcanic particle clusters
526 based on field and numerical investigations. J Volcanol Geotherm Res. 327, 520–530.
527 doi: 10.1016/j.jvolgeores.2016.09.009

528 Bonadonna C, Genco R, Gouhier M, et al. (2011) Tephra sedimentation during the 2010
529 Eyjafjallajökull eruption (Iceland) from deposit, radar, and satellite observations. J
530 Geophys Res 116, B12202. doi: 10.1029/2011JB008462

531 Brown RJ, Bonadonna C, Durant AJ (2012) A review of volcanic ash aggregation. Phys Chem
532 Earth 45–46:65–78. doi: 10.1016/j.pce.2011.11.001

533 Burns FA, Bonadonna C, Pioli L, et al. (2017) Ash aggregation during the 11 February 2010
534 partial dome collapse of the Soufriere Hills Volcano, Montserrat. J Volcanol Geotherm
535 Res 335:92–112. doi: 10.1016/j.jvolgeores.2017.01.024

536 Cole P, Guest J, Duncan A, et al. (2001) Capelinhos 1957-1958, Faial, Azores: deposits formed
537 by an emergent surtseyan eruption. Bull Volcanol 63:204–220. doi:
538 10.1007/s004450100136

539 Colombier M, Scheu B, Wadsworth FB, et al. (2018) Vesiculation and Quenching During
540 Surtseyan Eruptions at Hunga Tonga-Hunga Ha'apai Volcano, Tonga. J Geophys Res
541 Solid Earth 123:3762–3779. doi: 10.1029/2017JB015357

542 Colombier M, Scheu B, Kueppers U, et al. (2019) In situ granulation by thermal stress during
543 Subaqueous volcanic eruptions. Geology 47:179–182. doi:
544 10.1130/G45503.1/4607844/g45503

545 Costa A, Macedonio G, Folch A (2006) A three-dimensional Eulerian model for transport and
546 deposition of volcanic ashes. Earth Planet Sci Lett 241:634–647. doi:
547 10.1016/j.epsl.2005.11.019

548 Costa A, Folch A, Macedonio G (2010) A model for wet aggregation of ash particles in volcanic
549 plumes and clouds: 1. Theoretical formulation. J Geophys Res 115:1–14. doi:
550 10.1029/2009JB007175

551 Cronin, S. J., M. Brenna, I. E. M. Smith, et al (2017) New volcanic island unveils explosive
552 past, Eos, 98. doi: 10.1029/2017EO076589

553 Cronin SJ, Neall VE, Lecointre JA, et al. (2003) Environmental hazards of fluoride in volcanic
554 ash: A case study from Ruapehu volcano, New Zealand. J Volcanol Geotherm Res
555 121:271–291. doi: 10.1016/S0377-0273(02)00465-1

556 Damby DE, Peek S, Lerner AH, et al. (2018) Volcanic ash leachate chemistry from increased
557 2018 activity of Kīlauea Volcano, Hawaii: U.S. Geological Survey data release,
558 https://doi.org/10.5066/P98A07DC.

559 Del Bello E, Taddeucci J, Scarlato P, et al. (2015) Experimental investigation of the
560 aggregation-disaggregation of colliding volcanic ash particles in turbulent, low-humidity
561 suspensions. Geophys Res Lett 1068–1075. doi: 10.1002/2014GL062292

562 Delmelle P, Pelletier M (2005) Surface area, porosity and water adsorption properties of fine
563 volcanic ash particles. Bull Volcanol 67:160–169. doi: 10.1007/s00445-004-0370-x

564 Delmelle P, Lambert M, Dufrêne Y, et al. (2007) Gas/aerosol-ash interaction in volcanic plumes:
565 New insights from surface analyses of fine ash particles. Earth Planet Sci Lett 259:159–
566 170. doi: 10.1016/j.epsl.2007.04.052

567 Delmelle P, Wadsworth FB, Maters EC, et al. (2018) High Temperature Reactions Between
568 Gases and Ash Particles in Volcanic Eruption Plumes. Reviews in Mineralogy and
569 Geochemistry 84:285–308. doi: 10.2138/rmg.2018.84.8

570 Douillet GA, Tsang-Hin-Sun È, Kueppers U, et al. (2013) Sedimentology and geomorphology
571 of the deposits from the August 2006 pyroclastic density currents at Tungurahua volcano,
572 Ecuador. Bull Volcanol 75:765. doi: 10.1007/s00445-013-0765-7

573 Draxler RR, Hess GD (1997) Description of the HYSPLIT4 Modeling system. NOAA Tech
574 Mem ERL ARL-224.

575 Ennis BJ, Tardos G, Pfeffer R (1991) A microlevel-based characterization of granulation
576 phenomena. Powder Technol 65:257–272

577 Eychenne J, Le Pennec J-L, Troncoso L, et al (2012) Causes and consequences of bimodal
578 grain-size distribution of tephra fall deposited during the August 2006 Tungurahua
579 eruption (Ecuador). Bull Volcanol 74:187–205. doi: 10.1007/s00445-011-0517-5

580 Folch A, Costa A, Durant A, et al. (2010) A model for wet aggregation of ash particles in
581 volcanic plumes and clouds: 2. Model application. J Geophys Res 115:1–16. doi:
582 10.1029/2009JB007176

583 Garvin JB, Slayback DA, Ferrini V, et al. (2018) Monitoring and Modeling the Rapid Evolution
584 of Earth's Newest Volcanic Island: Hunga Tonga Hunga Ha'apai (Tonga) Using High
585 Spatial Resolution Satellite Observations. Geophys Res Lett 45:3445–3452. doi:
586 10.1002/2017GL076621

587 Gilbert JS, Lane SJ (1994) The origin of accretionary lapilli. Bull Volcanol 56:398–411. doi:
588 10.1007/BF00326465

589 Hoshyaripour G, Hort M, Langmann B (2014) Ash iron mobilization in volcanic eruption
590 plumes. Atmosph. Chem Phys Disc 14:32535–3258.

591 Hovland M, Rueslatten HG, Johnsen HK, et al. (2015) Salt formation associated with sub-
592 surface boiling and supercritical water. Mar Pet Geol 23:855–869. doi:
593 10.1016/j.marpetgeo.2006.07.002

594 James MR, Gilbert JS, Lane SJ (2002) Experimental investigation of volcanic particle
595 aggregation in the absence of a liquid phase. J Geophys Res 107:1–13. doi:
596 10.1029/2001JB000950

597 Kelfoun K, Samaniego P, Palacios P, et al. (2009) Testing the suitability of frictional behaviour
598 for pyroclastic flow simulation by comparison with a well-constrained eruption at
599 Tungurahua volcano (Ecuador). Bull Volcanol. doi: 10.1007/s00445-009-0286-6

600 Kueppers U, Ayris P, Bernard B, et al. (2016) Volcano vs. environment: Where, when and why
601 does ash aggregate? Cities on Volcanoes 9, November 2016, Puerto Varas, Chile

602 Kokelaar P (1986) Magma-water interactions in subaqueous and emergent basaltic volcanism.
603 Bull Volcanol 1:275–289

604 Lathem TL, Kumar P, Nenes A, et al. (2011) Hygroscopic properties of volcanic ash. Geophys
605 Res Lett 38:2–5. doi: 10.1029/2011GL047298

606 Mastin LG, Guffanti M, Servranckx R, et al. (2009) A multidisciplinary effort to assign realistic
607 source parameters to models of volcanic ash-cloud transport and dispersion during
608 eruptions. J Volcanol Geotherm Res 186:10–21. doi: 10.1016/j.jvolgeores.2009.01.008

609 Morgavi D, Valentini L, Porreca M, et al (2019) Volcanic ash aggregation enhanced by
610 seawater interaction : the case of the Secche di Lazzaro phreatomagmatic deposit (
611 Stromboli). Ann Geophys 61:. doi: 10.4401/ag-7874

612 Mueller SB, Kueppers U, Ayris PM, et al. (2016) Experimental volcanic ash aggregation:
613 Internal structuring of accretionary lapilli and the role of liquid bonding. Earth Planet Sci
614 Lett 433:232–240. doi: 10.1016/j.epsl.2015.11.007

615 Mueller SB, Ayris PM, Wadsworth FB, et al. (2017) Ash aggregation enhanced by deposition
616 and redistribution of salt on the surface of volcanic ash in eruption plumes. Scientific
617 reports, 7, 45762. doi: 10.1038/srep45762

618 Mueller SB, Kueppers U, Ametsbichler J, et al. (2017) Stability of volcanic ash aggregates and
619 break-up processes. Sci Rep 7:1–11. doi: 10.1038/s41598-017-07927-w

620 Mueller SB, Kueppers U, Huber MS, et al (2018) Aggregation in particle rich environments :
621 a textural study of examples from volcanic eruptions , meteorite impacts , and fluidized
622 bed processing. Bull Volcanol 80:32. doi: 10.1007/s00445-018-1207-3

623 Murata K., Dondoli C, Saenz R (1966) The 1963-65 Eruption of Irazti Volcano, Costa Rica
624 (The period of March 1963 to October 1964). Bull Volcanol 29:763

625 Neal CA, Brantley SR, Antolik L, et al (2018) The 2018 rift eruption and summit collapse of
626 Kīlauea Volcano. Science (80-) 363:367–374. doi: 10.1126/science.aav7046

627 Oskarsson N (1980) The interaction between volcanic gases and tephra: fluorine adhering to
628 tephra of the 1970 Hekla eruption. J Volcanol Geotherm Res 8:251-266.

629 Parkhurst DL, Appelo CAJ (1999) Users guide to PHREEQC (version 2) - a computer program
630 for speciation, reaction-path, 1D-transport, and inverse geochemical calculations. US
631 Geological Survey Water Resources Investigations Report 99–4259:312p

632 Rose WI (1977) Scavenging of volcanic aerosol by ash: atmospheric and volcanologic
633 implications. Geology 5:621–624.

634 Salman AD, Hounslow MJ, Seville JPK (2006) Handbook of Powder Technology –
635 Granulation, eleventh Ed. Elsevier, Amsterdam, 1402 p

636 Saxby J, Beckett F, Cashman K, et al. (2018) The impact of particle shape on fall velocity:
637 Implications for volcanic ash dispersion modelling. J Volcanol Geotherm Res 362:32–48.
638 doi: 10.1016/j.jvolgeores.2018.08.006

639 Scarlato P, Mollo S, Bello E Del, et al. (2016) The 2013 eruption of Chaparrastique volcano (El
640 Salvador): Effects of magma storage, mixing, and decompression. Chem Geol 448:110–
641 122. doi: 10.1016/j.chemgeo.2016.11.015

642 Schumacher R, Schmincke H (1991) Internal structure and occurrence of accretionary lapilli -
643 a case study at Laacher See Volcano. Bull Volcanol 53:612–634

644 Steffke AM, Fee D, Garces M, Harris A (2010) Eruption chronologies , plume heights and
645 eruption styles at Tungurahua Volcano : Integrating remote sensing techniques and
646 infrasound. J Volcanol Geotherm Res 193:143–160. doi:
647 10.1016/j.jvolgeores.2010.03.004

648 Stinton AJ, Cole PD, Stewart RC, et al. (2014) The 11 February 2010 partial dome collapse at
649 Soufriere Hills Volcano, Montserrat. Geol Soc London, Mem. 39(1), 133–152. doi:
650 10.1144/M39.7

651 Stumm W, Morgan JJ (1996) Aquatic Chemistry: Chemical Equilibria and Rates in Natural
652 Waters. John Wiley & Sons.

653 Taddeucci J, Scarlato P, Montanaro C, et al. (2011) Aggregation-dominated ash settling from
654 the Eyjafjallajökull volcanic cloud illuminated by field and laboratory high-speed
655 imaging. Geology 39:891–894. doi: 10.1130/G32016.1

656 Taylor PS, Stoiber RE (1973) Soluble Material on Ash from Active Central American
657 Volcanoes. Geol Soc Am Bull 84:1031–1042

658 Van Eaton AR, Muirhead JD, Wilson CJN, et al. (2012) Growth of volcanic ash aggregates in
659 the presence of liquid water and ice: an experimental approach. Bull Volcanol 74:1963–
660 1984. doi: 10.1007/s00445-012-0634-9

661 Witham CS, Oppenheimer C, Horwell CJ (2005) Volcanic ash-leachates: A review and
662 recommendations for sampling methods. J Volcanol Geotherm Res 141:299–326. doi:
663 10.1016/j.jvolgeores.2004.11.010

Wright HMN, Cashman K V, Mothes PA, et al (2012) Estimating rates of decompression from textures of erupted ash particles produced by 1999 – 2006 eruptions of Tungurahua volcano , Ecuador. Geology 40:619–622. doi: 10.1130/G32948.1

668 **Tables and figure captions**

669

670 **Table1.** Results from the leaching analysis showing the concentrations of anions and single
671 elements in ppm.

672

673 **Figure 1.** Concentrations in ppm of Na, Cl^-, Ca, $SO4^{2-}$, K and Mg in aggregates from Hunga
674 Tonga-Hunga Ha'apai, Soufrière Hills, Tungurahua and Chaparrastique. For Hunga Tonga-
675 Hunga Ha'apai, a range is given for each ion. The dashed blue line corresponds to the highest
676 Cl^- content previously found in the literature in ash samples from Irazú volcano, Costa Rica
677 (Taylor and Stoiber, 1973). The grey field corresponds to the range for the highest SO_4^{2-}
678 concentrations found at Ruapehu (Cronin et al., 2003) and Kilauea (Damby et al., 2018).

679

680 **Figure 2.** SEM BSE images and chemical mapping revealing the presence of NaCl and $CaSO_4$
681 in the ash rims of lapilli from sample HH33. a to e: Large $CaSO_4$ salt (in blue) and Cl bearing
682 salts visible in the Cl elemental map in (e). f to i: Large NaCl salt (in green) and smaller $CaSO_4$
683 salts (in blue).

684

685 **Figure 3.** Correlations between the molar concentrations of Na-Cl and Ca-SO_4 revealing an
686 approximately 1:1 relationship implying the presence of salts NaCl and $CaSO_4$ in the ash rims
687 prior to leaching.

688

689 **Figure 4.** Evolution of the saturation state of seawater with respect to carbonate, sulfate and
690 chloride salts during evaporation. The amount of different salts as a function of the
691 concentration factor (a) and the degree of evaporation (b) are shown.

692

693 **Figure 5.** Evolution of concentrations in Cl^-, Na, Ca and SO_4^{2-} analyzed in the aggregates from
694 Hunga Tonga-Hunga Ha'apai as a function of their position in the stratigraphic sequence of the
695 cone-building phase.

696

Figure 6. Schematic representation of the spectrum of natural volcanic settings for salt precipitation considered in our study and expected salt concentrations. Subaerial eruptions with massive degassing, presence of a crater lake and hydrothermal activity are not shown in this diagram but also represent natural settings with extensive salt formation.

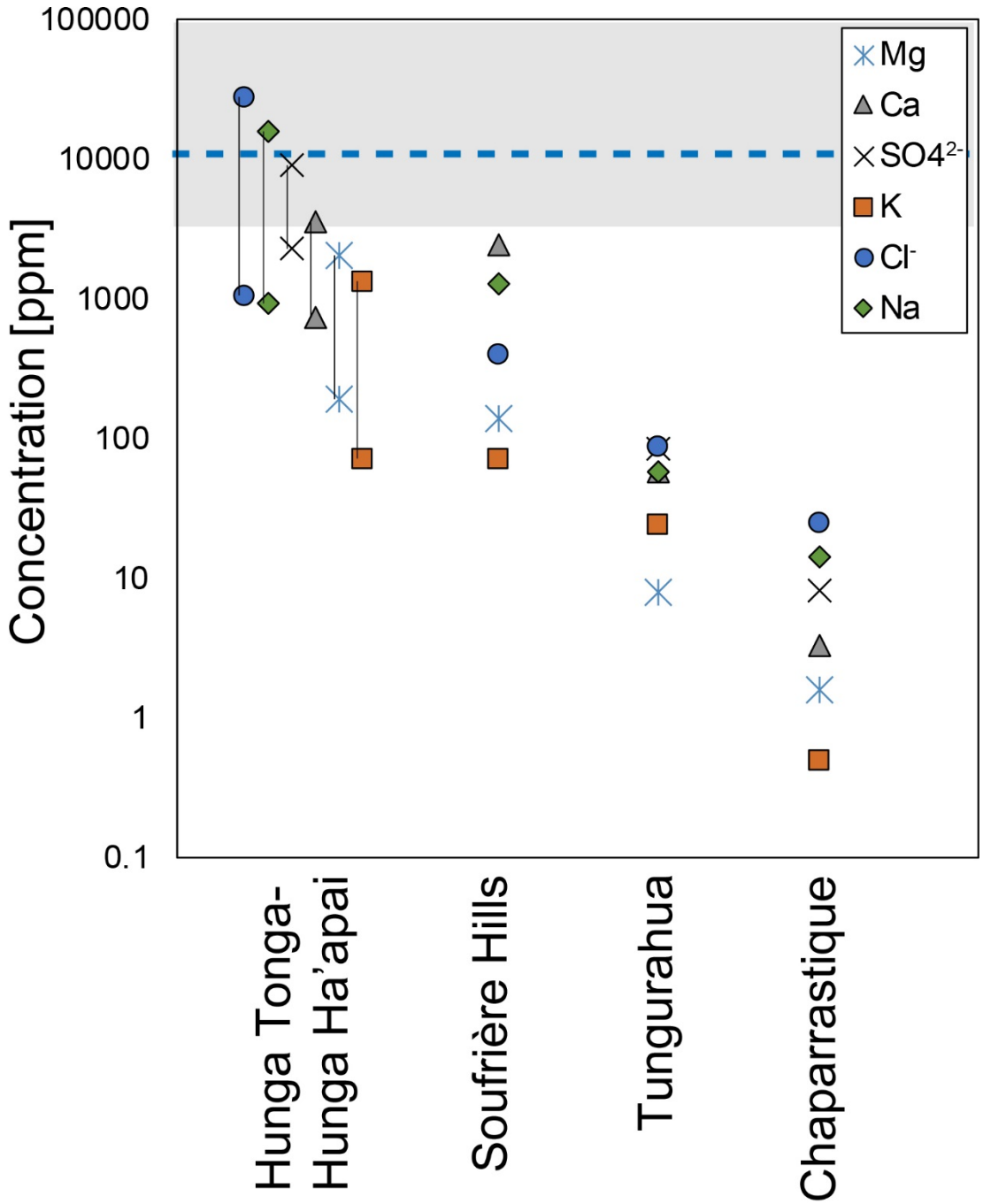

706

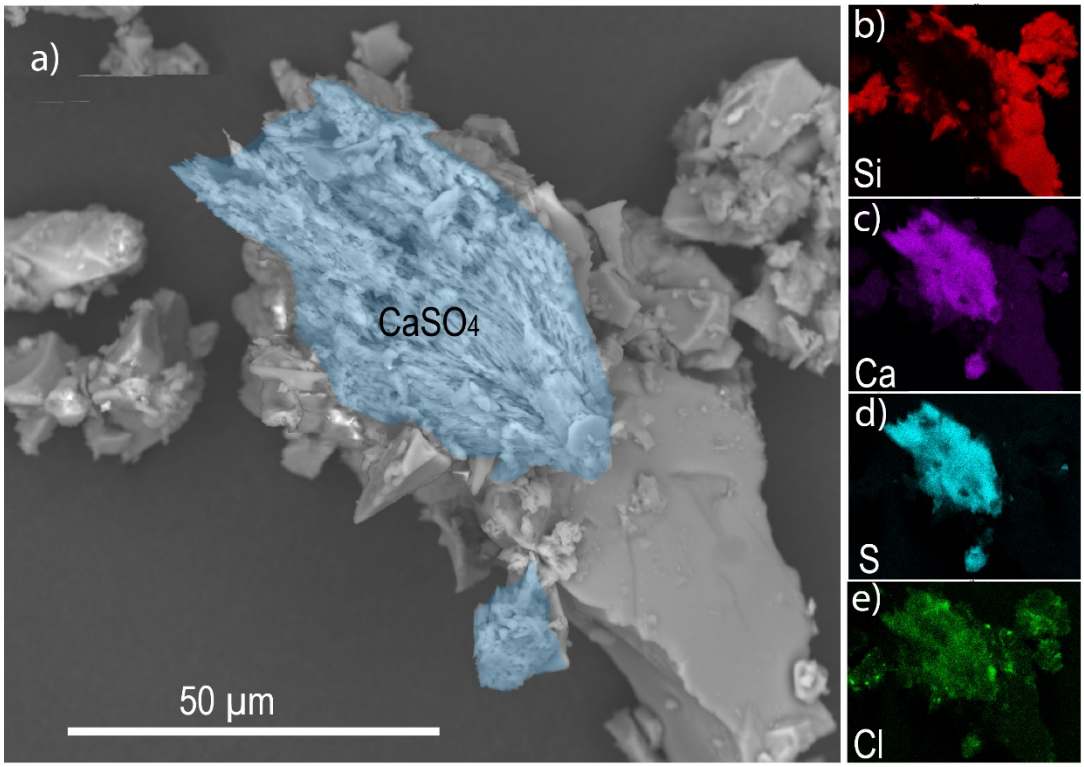

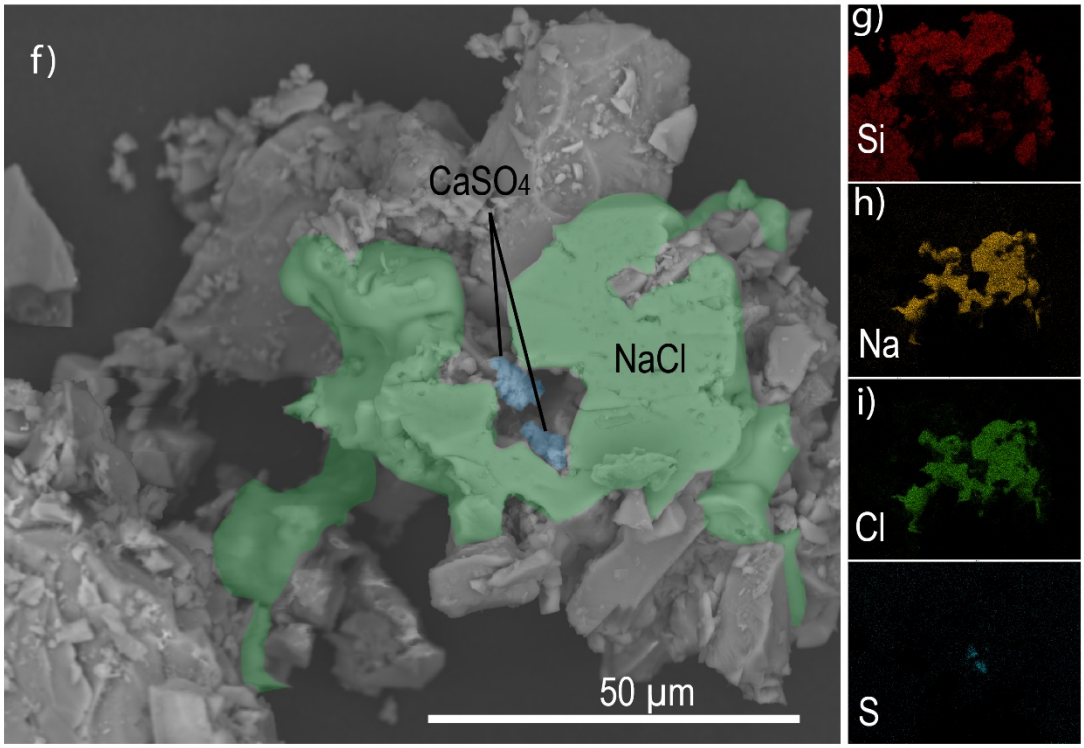

707

708

709

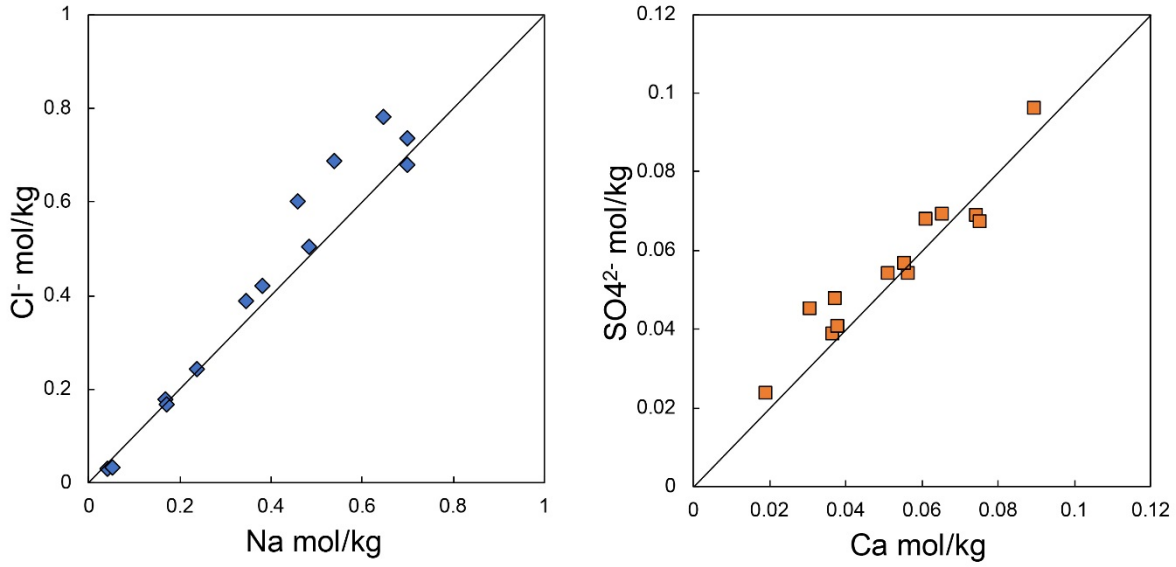

710

711

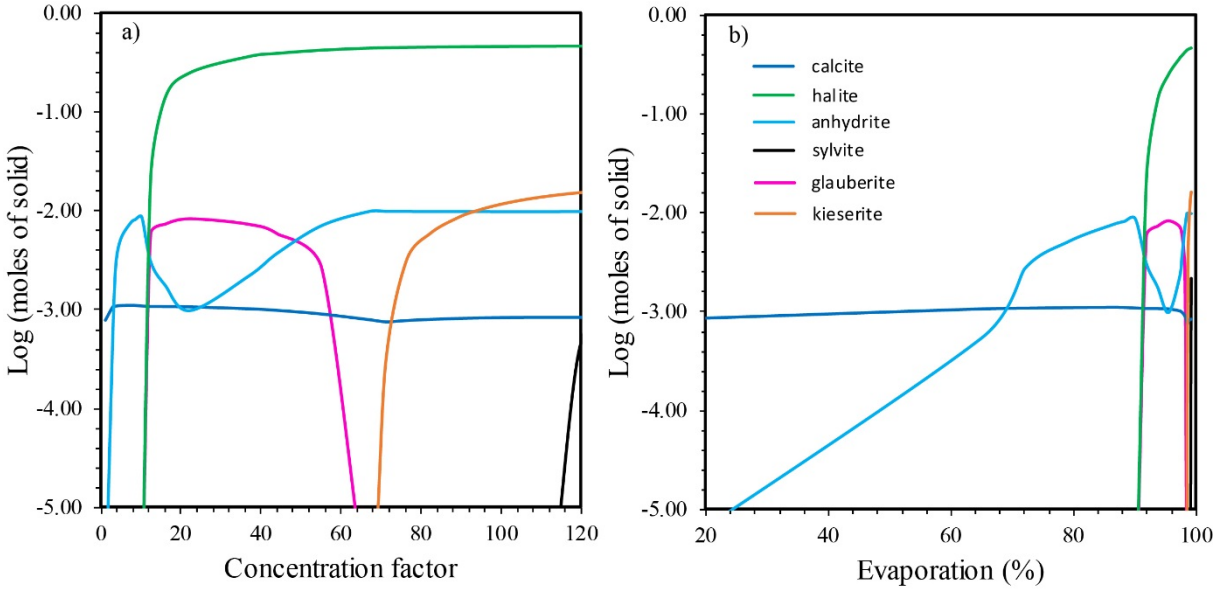

712

713

714

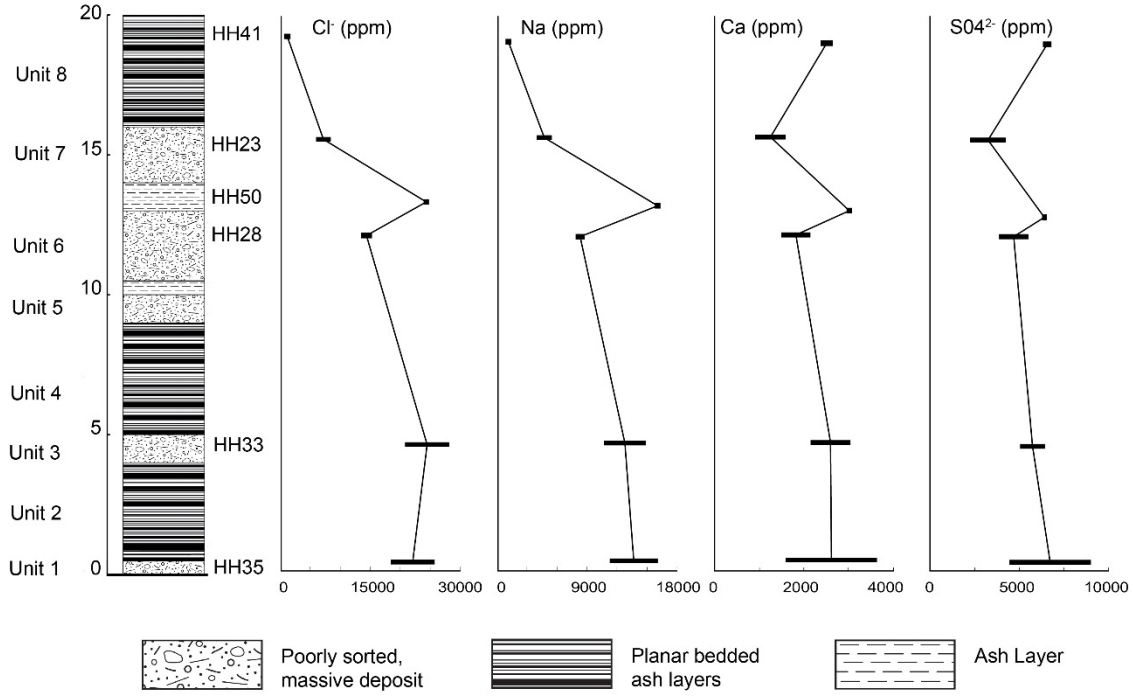
20
15
10
5
0
Unit 8
Unit 7
Unit 6
Unit 5
Unit 4
Unit 3
Unit 2
Unit 1
HH41
HH23
HH50
HH28
HH33
HH35
Cl- (ppm)
0
15000
30000
Na (ppm)
0
9000
18000
Ca (ppm)
0
2000
4000
S04 2- (ppm)
0
5000
10000
Poorly sorted, massive deposit
Planar bedded ash layers
Ash Layer

715

716

717

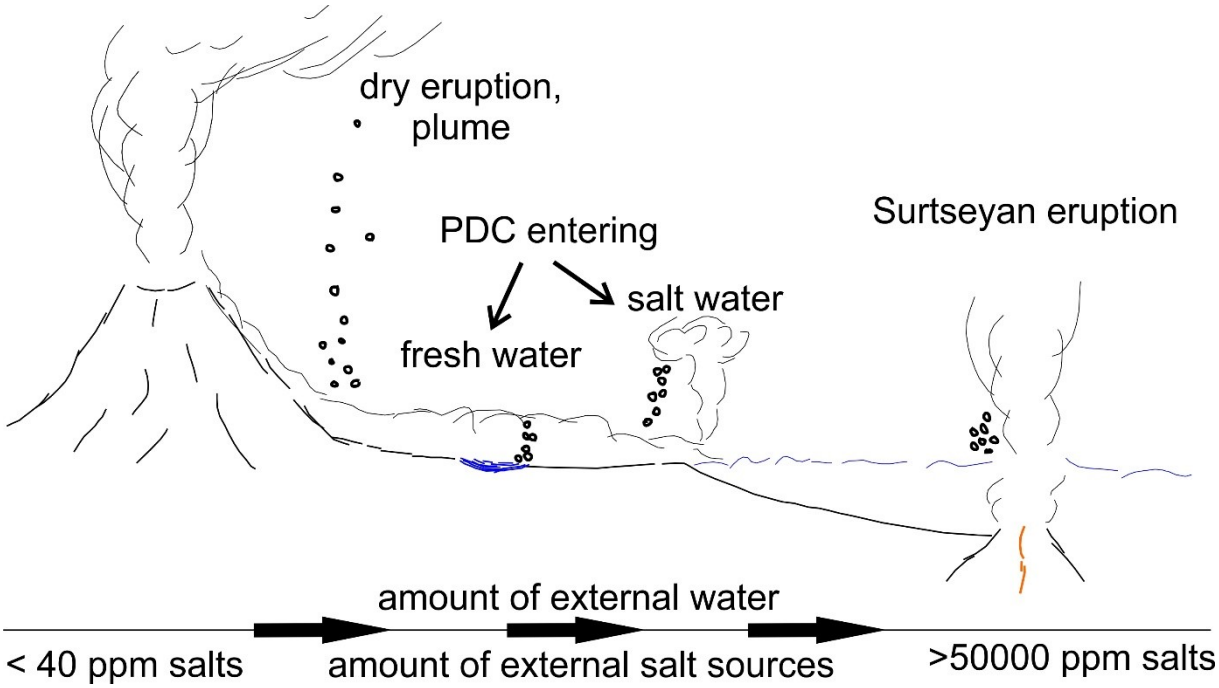

718

719

720

Study	Volcano	Type	Dilution ratio	Sample	Si	Mg	Ca	Na	K	Mn	Cl^-	$SO4^{2-}$
									[ppm]			
This study	Hunga Tonga- Hunga Ha'apai, Tonga	aggregates	1:100	23	725	321	753	3828	164	14	6325	2291
	Hunga Tonga- Hunga Ha'apai, Tonga	aggregates	1:500	23	3551	351	1451	5420	164	17	8605	3733
	Hunga Tonga- Hunga Ha'apai, Tonga	aggregates	1:1000	23	7255	323	1215	3939	153	17	5879	4344
	Hunga Tonga- Hunga Ha'apai, Tonga	aggregates	1:500	41	-	194	2425	932	72	-	1060	6511
	Hunga Tonga- Hunga Ha'apai, Tonga	aggregates	1:1000	41	-	210	2600	1188	78	-	1182	6650
	Hunga Tonga- Hunga Ha'apai, Tonga	aggregates	1:500	50	-	1727	3000	16070	1325	-	24099	6450
	Hunga Tonga- Hunga Ha'apai, Tonga	aggregates	1:100	33	1597	1817	2034	14850	530	53	27703	5200
	Hunga Tonga- Hunga Ha'apai, Tonga	aggregates	1:500	33	7740	1940	2249	10555	589	60	21270	5202
	Hunga Tonga- Hunga Ha'apai, Tonga	aggregates	1:1000	33	14900	2049	2956	12350	593	73	24332	6601
	Hunga Tonga- Hunga Ha'apai, Tonga	aggregates	1:1000	35	7185	1201	3563	16060	436	25	26082	9230
	Hunga Tonga- Hunga Ha'apai, Tonga	aggregates	1:1000	35	7308	657	1485	11070	242	16	17814	4599
	Hunga Tonga- Hunga Ha'apai, Tonga	aggregates	1:500	28	-	676	1500	7920	239	-	13732	3919
	Hunga Tonga- Hunga Ha'apai, Tonga	aggregates	1:1000	28	-	768	2200	8725	303	-	14902	5455
	Soufrière Hills, Montserrat	aggregates	1:500		-	140	2462	1297	72	-	400	-
	Tungurahua, Ecuador	aggregates	1:500		-	8	58	58	24	-	88	85
	Chaparrastique, El Salvador	aggregates	1:500		-	2	3	14	1	-	25	8
	Soufrière Hills, Montserrat	non-aggregated material	1:500			31	1395	218	14	-	85	-
	Tungurahua, Ecuador	non-aggregated material	1:500			4	40	37	11	-	49	86
Whitham et al., 2005	Compilation					-	-	-	-	-	4-11160	2-21775
Ayris and Delmelle, 2012	Compilation					<1-4240	<1-23590	<1-2560	<1-788	<1-144	-	-
Cronin et al., 2003	Ruapehu											1800-31000
		seawater concentrations				1272	400	10561	380	0.01	18980	2712

721